

# Formation and Early Evolution of Circumstellar Disks in Turbulent Molecular Cloud Cores

Yusuke Tsukamoto<sup>1,2</sup> and Masahiro N. Machida<sup>3</sup>

<sup>1</sup>*Department of Astronomy, the University of Tokyo, Hongo 7-3-1, Bunkyo-ku, Tokyo, Japan*

<sup>2</sup>*Division of Theoretical Astronomy, National Astronomical Observatory of Japan, 2-21-1 Osawa, Mitaka, Tokyo, Japan*

<sup>3</sup>*Department of Earth and Planetary Sciences, Kyushu University, 6-10-1 Hakozaki, Higashi-ku, Fukuoka, Fukuoka, Japan*

5 August 2021

## ABSTRACT

We investigate the formation and evolution of circumstellar disks in turbulent cloud cores until several  $10^4$  years after protostar formation using smoothed particle hydrodynamics (SPH) calculations. The formation and evolution process of circumstellar disk in turbulent cloud cores differs substantially from that in rigidly rotating cloud cores. In turbulent cloud cores, a filamentary structure appears before the protostar formation and the protostar forms in the filament. If the turbulence is initially sufficiently strong, the remaining filament twists around the protostar and directly becomes a rotation-supported disk. Upon formation, the disk orientation is generally misaligned with the angular momentum of its host cloud core and it dynamically varies during the main accretion phase, even though the turbulence is weak. This is because the angular momentum of the entire cloud core is mainly determined by the large scale velocity field whose wavelength is comparable to the cloud scale, whereas the angular momentum of the disk is determined by the local velocity field where the protostar forms and these two velocity fields do not correlate with each other. In the case of disk evolution in a binary or multiple stars, the disks are misaligned with each other at least during the main accretion phase, because there is no correlation between the velocity fields around the position where each protostar forms. In addition, each disk is also misaligned with the binary orbital plane. Such misalignment can explain the recent observations of misaligned disks and misaligned protostellar outflows.

**Key words:** star formation – circumstellar disk – protoplanetary disk – planet formation – binary system – methods: hydrodynamics – smoothed particle hydrodynamics

## 1 INTRODUCTION

Many circumstellar disks are observed in star-forming regions. They are by-products of star formation and are directly connected to planet formation. Thus, it is important for understanding star and planet formation to clarify the formation and evolution of circumstellar disks. Recent studies on protostar and disk formation in a collapsing molecular cloud core suggest that the circumstellar disk forms at a very early phase of star formation (Bate 1998; Walch et al. 2009; Machida et al. 2010; Inutsuka et al. 2010; Bate 2011), and is more massive than the protostar for at least  $10^4$  years after protostar formation (Inutsuka et al. 2010). During this phase, the circumstellar disk is gravitationally unstable and develops non-axisymmetric spiral arms. However, these studies have examined the formation and evolution of the circumstellar disk in the rigidly rotating cloud core.

Molecular clouds, which typically have a scale  $> 0.1$  pc, usually display complex internal motions that are observed

as a broad emission-line profile. The internal motion in a molecular cloud is believed to be caused by turbulence. Although a detailed generation process of the internal motions is still unclear, observed line profiles in molecular clouds are consistent with Gaussian velocity fields with a Kolmogorov spectrum (Dubinski et al. 1995; Klessen 2000). Observations also indicate the existence of turbulence even for molecular cloud cores, which typically have a scale of 0.1–0.01 pc. Goodman et al. (1993) showed that the specific angular momentum of a molecular cloud core is roughly proportional to  $j \propto R^{1.6}$ , which is derived from observations of molecular cloud cores with a size of 0.06 – 0.6 pc. This scaling law is in good agreement with the scaling,  $j \propto R^{1.5}$  which is produced by a turbulence field with velocity power spectrum,  $P(k) \propto k^{-4}$ . Note that when the molecular cloud core rotates rigidly, the specific angular momentum should obey the scaling law of  $j \propto R^2$ . Burkert & Bodenheimer (2000) pointed out that random Gaussian velocity fields with power

spectra of  $P(k) \propto k^{-4}$  can reproduce the observed projected rotational properties of molecular cloud cores.

The evolution of a circumstellar disk during Class 0–I phases may be strongly affected by the velocity field of the molecular cloud core because it is mainly determined by mass accretion from the (turbulent) envelope. Thus, it is important to investigate the disk evolution in turbulent molecular cloud cores for a comprehensive understanding of the evolution of circumstellar disks.

In addition to formation and evolution of the circumstellar disk around a single protostar, cloud turbulence is also expected to affect the formation and evolution of circumstellar disks in binary systems. In a collapsing cloud core, fragmentation may occur, causing a binary system to appear. In a rigidly rotating cloud core, disks in the binary system are aligned with each other by definition and also with the binary orbital plane (see, Tsukamoto & Machida 2011). On the other hand, observational evidence indicates misalignment of binary disks. For example, Davis et al. (1994) observed protostellar jets with different orientations in a binary system. Roccatagliata et al. (2011) recently observed two disks in a proto-binary system. In their observation, the primary protostar has an almost face-on disk, whereas the secondary disk is edge-on toward the observer. Thus, the disk orientation around the primary protostar is almost perpendicular to the orientation of the disk around the secondary protostar. With observations of many wide binary systems, Hale (1994) showed that the stellar rotational equatorial plane is often misaligned with the binary orbital plane. These observations indicate that in wide binary systems, the disk plane is frequently misaligned with the binary orbital plane. However, simulations starting from a molecular cloud core with simple systematic rotation cannot explain these observations.

The gravitational collapse of a turbulent molecular cloud core has been studied by several groups. Matsumoto & Hanawa (2011) calculated the gravitational contraction of turbulent cloud cores and showed the morphological evolution of the collapsing cloud core before protostar formation. With long term calculations (until  $\sim 10^5$  years after the protostar formation), Goodwin et al. (2004b,a) showed that fragmentation frequently occurs even in a weakly turbulent environment. Recently, Walch et al. (2010) calculated the evolution of turbulent cloud cores and showed that protostar and circumstellar disk formation in turbulent cloud cores is different from that in rigidly rotating cloud cores. They showed that protostars form from a filamentary structure and pointed out that the formation condition for a binary or multiple stellar system rarely depends on the total angular momentum of the host cloud core. Walch et al. (2012) investigated the evolution of low-mass cold cores. They focused on the relationship between the evolution of the core and the maximum wavelength (or minimum wavenumber) of the turbulence and found that the maximum wavelength of the turbulence is a critical parameter for the evolution of cloud cores. In their simulation, the turbulent energy is fixed and the dependence of the disk evolution on the turbulent energy is still unclear.

In this study, we investigate circumstellar disk formation in a turbulent cloud core over  $> 10^4$  years. We have already reported the disk formation in cloud cores with systematic rotation (or rigid rotation) in

Tsukamoto & Machida (2011) in which we calculated the cloud evolution with different classical cloud parameters (e.g., Miyama et al. 1984) representing the cloud thermal ( $\alpha$ ) and rotational ( $\beta$ ) energies. In the present study, which is complementary to that of Tsukamoto & Machida (2011), we investigate the effects of turbulence strength on the evolution of the protostar and circumstellar disk with one cloud parameter representing thermal ( $\alpha$ ) energy and one representing turbulent ( $\gamma_{\text{turb}}$ ) energy. We also investigate disk evolution and its orientation in a binary system. This paper is organized as follows. In §2, we describe the numerical method and initial conditions. In §3, we present the numerical results. Finally, in §4, we discuss our results.

## 2 NUMERICAL METHOD AND INITIAL CONDITIONS

### 2.1 Numerical Method

Our simulations were conducted using the smoothed particle hydrodynamics (SPH) code, which we used in our previous study (Tsukamoto & Machida 2011). The code includes an individual time-step technique and uses the Barnes-Hut tree algorithm to calculate the self-gravity with an opening angle  $\theta = 0.5$ . We include an artificial viscosity according as prescribed by Monaghan (1997) with  $\alpha_v = 1$  and also use the Balsara switch (Balsara 1995). Our code was parallelized with MPI and was verified using several standard test problems.

To mimic the thermal evolution of the cloud core calculated by Masunaga & Inutsuka (2000), we adopted the following barotropic equation of state,

$$P = c_{s,0}^2 \rho \left[ 1 + \left( \frac{\rho}{\rho_c} \right)^{2/5} \right], \quad (1)$$

where  $c_{s,0} = 190 \text{ m s}^{-1}$  and  $\rho_c = 4 \times 10^{-14} \text{ g cm}^{-3}$ .

In addition, to calculate the evolution of the circumstellar disk for  $\gtrsim 10^4$  years, we adopted the sink particle technique described by Bate et al. (1995). We assume that a protostar forms when the particle density exceeds the threshold density,  $\rho_{\text{sink}} = 4 \times 10^{-9} \text{ g cm}^{-3}$ . Next, a sink particle with an accretion radius of 1 AU is dynamically introduced.

### 2.2 Initial Settings

As the initial state, we adopt a spherically-symmetric cloud core with an isothermal temperature of  $T = 10 \text{ K}$ . Each cloud core has a uniform density within the range  $\rho_{\text{init}} = 6.9 \times 10^{-19}$  to  $1.9 \times 10^{-17} \text{ cm}^{-3}$  and a size ranging from  $R = 1967$  to  $5900 \text{ AU}$  (see, Table 1). All models have the same cloud mass of  $1 M_{\odot}$ . The initial cloud cores are modeled with about 520000 SPH particles. The mass resolution of all calculations is  $1.9 \times 10^{-6} M_{\odot}$  and our calculations fulfill the resolution requirement suggested by Bate & Burkert (1997). The smoothing length of  $i$  th particle,  $h_i$  is given as

$$h_i = 1.2 \left( \frac{m_i}{\rho_i} \right)^{1/3}, \quad (2)$$

where  $m_i$ ,  $\rho_i$  are the mass and the density of  $i$  th particle. Only a turbulent velocity field without the systematic rotation velocity is imposed on the initial cloud core.

**Table 1.** Model parameters

Model	$\alpha$	$\gamma_{\text{turb}}$	$R$ (AU)	$\beta_{\text{eff}}$	$\rho_{\text{init}}$ (g cm $^{-3}$ )	Mach number <sup>1</sup>	Fragmentation
1	0.6	0.1	5900	$1.3 \times 10^{-2}$	$6.9 \times 10^{-19}$	0.66	N
2	0.6	0.06	5900	$7.9 \times 10^{-3}$	$6.9 \times 10^{-19}$	0.50	N
3	0.6	0.03	5900	$4.1 \times 10^{-3}$	$6.9 \times 10^{-19}$	0.36	N
4	0.4	0.3	3933	$4.1 \times 10^{-2}$	$2.3 \times 10^{-18}$	1.4	N
5	0.4	0.1	3933	$1.4 \times 10^{-2}$	$2.3 \times 10^{-18}$	0.80	N
6	0.4	0.06	3933	$8.5 \times 10^{-3}$	$2.3 \times 10^{-18}$	0.63	N
7	0.2	0.3	1967	$4.0 \times 10^{-2}$	$1.9 \times 10^{-17}$	2.0	Y
8	0.2	0.1	1967	$1.3 \times 10^{-2}$	$1.9 \times 10^{-17}$	1.1	Y
9	0.2	0.06	1967	$8.2 \times 10^{-3}$	$1.9 \times 10^{-17}$	0.87	Y

<sup>1</sup> Mach number is the root mean square of the turbulent velocity in the initial cloud core.

### 2.2.1 Model Parameters

Gas accretion from the infalling envelope onto the circumstellar disk controls the evolution of the circumstellar disk. The gas accretion rate is related to the thermal and kinetic (or turbulent) energies of the host cloud core. In this study, to investigate disk evolution in cloud cores with different thermal and turbulent energies, we use two parameters,  $\alpha$  and  $\gamma_{\text{turb}}$ . The parameter  $\alpha$  is the ratio of thermal energy ( $E_{\text{thermal}}$ ) to gravitational energy ( $E_{\text{grav}}$ ) in the initial cloud core and given as

$$\alpha = \frac{E_{\text{thermal}}}{|E_{\text{grav}}|} = \frac{5R_0c_{s,0}^2}{2GM}, \quad (3)$$

where  $R_0$  and  $M$  are the initial radius and mass of the cloud core, respectively. The parameter  $\gamma_{\text{turb}}$  is the ratio of turbulent energy ( $E_{\text{turb}}$ ) to gravitational energy ( $E_{\text{grav}}$ ):

$$\gamma_{\text{turb}} = \frac{E_{\text{turb}}}{|E_{\text{grav}}|}. \quad (4)$$

In equation (4),  $E_{\text{turb}}$  and  $E_{\text{grav}}$  are numerically estimated in the initial cloud core. The strength of the turbulent velocity field in the initial cloud core can be described by the parameter  $\gamma_{\text{turb}}$ .

### 2.2.2 Turbulence Realization

Burkert & Bodenheimer (2000) showed that random Gaussian velocity fields with power spectra of  $P(k) \propto k^{-3}$  to  $k^{-4}$  can reproduce the observed projected rotational properties of molecular cloud cores. Thus, a molecular cloud core apparently has a systematic rotation even when it has only a turbulent velocity field. We adopt a turbulent velocity field with power spectra of  $P(k) \propto k^{-4}$ , in which we assume a divergence-free velocity field. The prescription for realizing turbulence in our initial settings is as follows: First, we generate a random Gaussian field with the power spectrum  $P_A(k) \equiv |A_k|^2 \propto k^{-6}$ . Next, we compute the Fourier transform of the velocity field  $\mathbf{v}_k$  as

$$\mathbf{v}_k = i\mathbf{k} \times \mathbf{A}_k. \quad (5)$$

Finally, the velocity field is generated on a  $128^3$  uniform grid, and the particle velocities are interpolated from the grid. We adopted the minimum wave number to be  $k_{\text{min}} = 1$  and the maximum wave number to be  $k_{\text{max}} = 128$ . Unlike a rigidly rotating cloud core, the turbulent velocity field is

not uniquely identified by the parameter set,  $(\alpha, \gamma_{\text{turb}})$  because of its stochastic nature. Thus, it is difficult to systematically investigate the evolution of the turbulent cloud core with parameters  $\gamma_{\text{turb}}$  and  $\alpha$ . Goodwin et al. (2004a) and Walch et al. (2012) resolved this difficulty by considering the ensemble of simulations. Although their approach may be advantageous for investigating the turbulent cloud core, it requires too many computational resources. Therefore, we adopted a different approach for this study in which we simulate the evolution of the turbulent cloud core having a "typical" angular momentum for each parameter set. To construct a velocity field with typical angular momentum for a given parameter set  $(\alpha, \gamma_{\text{turb}})$ , we generated 1000 different velocity fields for each parameter set with different random number seeds. Next, from the 1000 velocity fields, we selected the velocity field whose angular momentum was the closest to the mean value of the angular momentum and used it to calculate the cloud evolution. This procedure makes it possible to simulate a turbulent cloud core that has a plausible angular momentum for a given parameter  $(\alpha, \gamma_{\text{turb}})$ . To relate the turbulent energy to the rotational energy of the initial cloud core, we introduce the parameter  $\beta_{\text{eff}}$  as

$$\beta_{\text{eff}} = \frac{25}{12} \frac{J_{\text{cloud}}^2}{GM^3R}, \quad (6)$$

where  $J_{\text{cloud}}$  is the total angular momentum of the cloud core. This parameter can be regarded as the effective ratio of rotational energy to gravitational energy of the cloud core. The values of  $\beta_{\text{eff}}$  for each model are listed in Table 1. According to this definition, the effective rotational energy is roughly related to the turbulent energy as  $\beta_{\text{eff}} \sim 0.1\gamma_{\text{turb}}$ .

Using the parameters  $\alpha$  and  $\gamma_{\text{turb}}$ , we constructed 9 models and calculated the evolution of the circumstellar disk for each model. The model names and parameters are listed in Table 1.

Note that we adopted the turbulent velocity field but the uniform density field as the initial state. Thus, the velocity field and density field of our initial conditions are not self-consistent. We will discuss how this inconsistency would affect our results in §4.5.1.

Note also that some models have somewhat unrealistic parameter. Model 7 have large initial Mach number that is much larger than typically observed and model 8 and 9 is highly gravitationally unstable ( $\alpha + \gamma_{\text{turb}} = 0.26, 0.3$ ). We will discuss the validity of these initial conditions in §4.5.2.

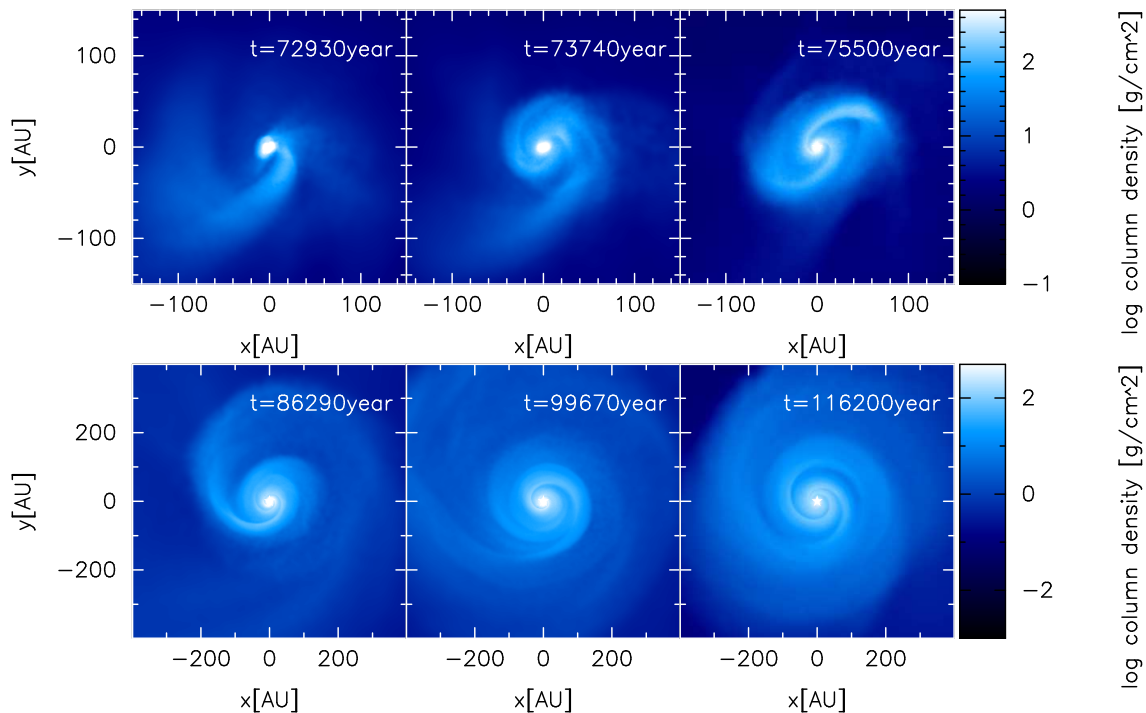


**Figure 1.** Time sequence of the logarithm of the face-on surface density before and after protostar formation for model 4 ( $\alpha = 0.4$  and  $\gamma_{\text{turb}} = 0.3$ ). The  $z$ -axis (i.e., the line-of-sight direction) is set parallel to the angular momentum of the entire initial cloud core. The top-left and -middle panels show snapshots approximately  $2.6 \times 10^3$  and  $1.8 \times 10^3$  years before protostar formation, respectively. The top-right panel shows a snapshot just when the protostar forms. The bottom left, -middle, and -right panels show snapshots  $1.1 \times 10^4$ ,  $2.1 \times 10^4$ , and  $4.1 \times 10^4$  years after protostar formation, respectively. The elapsed time in the calculation is shown in each panel.

### 3 RESULTS

In this section, we first give an overview of evolution process of circumstellar disk in turbulent core and how it changes in response to the strength of turbulence. We adopt model 4 ( $\alpha = 0.4$  and  $\gamma_{\text{turb}} = 0.3$ ) as a typical model with strong turbulence and model 6 ( $\alpha = 0.4$  and  $\gamma_{\text{turb}} = 0.06$ ) as a typical model with weak turbulence, and investigate them both in detail. It is observed that whether the initial velocity field is supersonic ( $M > 1$ ) or subsonic ( $M < 1$ ) is not important for the evolution processes. Next, we investigate the evolution of the disk orientation for all models and, finally, we investigate the formation process of binary or multiple systems in a turbulent cloud core and the evolution process of circumstellar disks in a binary system.

#### 3.1 Overview

##### 3.1.1 Disk evolution in strong turbulent core

In this subsection, we show how the circumstellar disk evolves in a turbulent cloud core that initially has relatively strong turbulence. As a typical case, we chose model 4 with parameters  $\alpha = 0.4$  and  $\gamma_{\text{turb}} = 0.3$  and an initial root mean square (rms) Mach number of 1.4. Figure 1 shows the time evolution of the surface density around the center of the cloud core. In the figure, the  $z$ -axis is chosen to be parallel to the angular momentum of the entire initial cloud core.

Before protostar formation, the first (adiabatic) core (Larson 1969; Masunaga & Inutsuka 2000) appears. The central region of high-density gas in the top-left and -middle

panels of Figure 1 corresponds to the first core. These panels show that filamentary structure accompanies the first core, which then, coils around the first core and changes directly to a circumstellar disk. The second collapse occurs at  $t = 75500$  years (top-right panel). By this epoch, the two spiral arms already develop. Although we cannot recognize the filamentary structure in the top-right panel, a weak large-scale filament remains around the disk at this epoch. In addition, the gas accretion from the filamentary structure onto the disk continues. After protostar formation, this large-scale filament (the structure which resides at  $\sim 200$  AU) coils around the disk and directly connects to the disk's spiral arm (bottom-left panel). Finally, as seen in the bottom-right panel of Figure 1, the filamentary structure accretes onto the disk and disappears.

Previous studies, which assumed the rigidly rotating cloud core with large rotational energy ( $\beta$  of the rigidly rotating core is comparable to  $\beta_{\text{eff}}$  of the turbulent core), have shown that the first core has enough angular momentum to develop a bar-mode instability and trailing spiral arms appears. The spiral arms remove the angular momentum from the central region. With the angular momentum transfer, the central density becomes high and the second collapse occurs. Then, the remnant of the first core which increases in size with the spiral arms becomes a circumstellar disk. (Bate 1998, 2011; Machida & Matsumoto 2011). However, the disk formation mechanism seen in Figure 1 differs from that found in the previous studies.

The first core formed in the turbulent cloud core has less angular momentum than that formed in the rigidly ro-

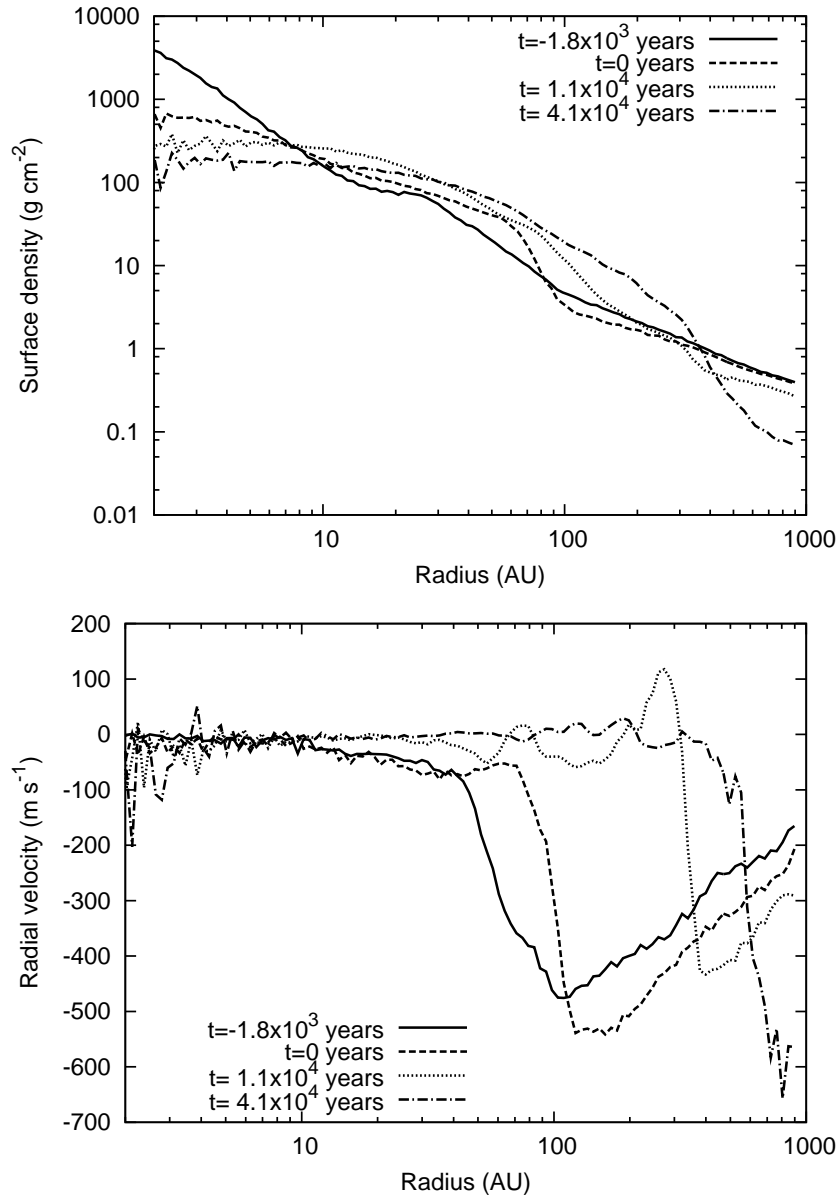


**Figure 2.** Radial distribution of surface density (top) and radial velocity (bottom) for model 4. Lines corresponds to  $1.8 \times 10^3$  years (solid line) before protostar formation, 0 years (dashed line),  $1.1 \times 10^4$  years (dotted line), and  $4.1 \times 10^4$  years (dashed-dotted line) after protostar formation.

tating cloud core because the gravitational collapse tends to occur at a stagnation point of the velocity field around which the rotational energy of the gas is relatively low. As a result, the first core cannot develop the bar-mode instability even with the strong turbulence. Instead, the filamentary structure, which forms before the first core formation, twists around the first core or protostar and, then, becomes directly a rotationally supported disk.

Figure 2 shows the radial profiles of the surface density and the radial velocity, for which each value is azimuthally averaged. The origin is set at the position of the protostar (or the position of the gas particle that has maximum density before the second collapse). The velocity is measured in the standard of rest of the protostar. The solid line in the top panel shows the surface density profile  $\sim 1.8 \times 10^3$

years before the second collapse, which corresponds to the top-middle panel of Figure 1. At this epoch, the disk surrounding the first core ranges from 10 to 50 AU. As described above, the filamentary structure, which formed before protostar formation, changes directly into the disk. The dashed line in the top panel of Figure 2 is the surface density profile at which the second collapse just begins. The disk radius reaches  $\sim 100$  AU at this epoch. The dotted line shows the surface density profile at  $\sim 1.1 \times 10^4$  years after the second collapse. At this epoch, as seen in the bottom panel of Figure 2, a positive radial velocity arises at approximately 200 to 300 AU. This flow is caused by the strong  $m = 1$  mode of the spiral arm which is generated approximately 100 AU. This type of outward flow appears repeatedly and readjust the surface density toward the stable configuration.

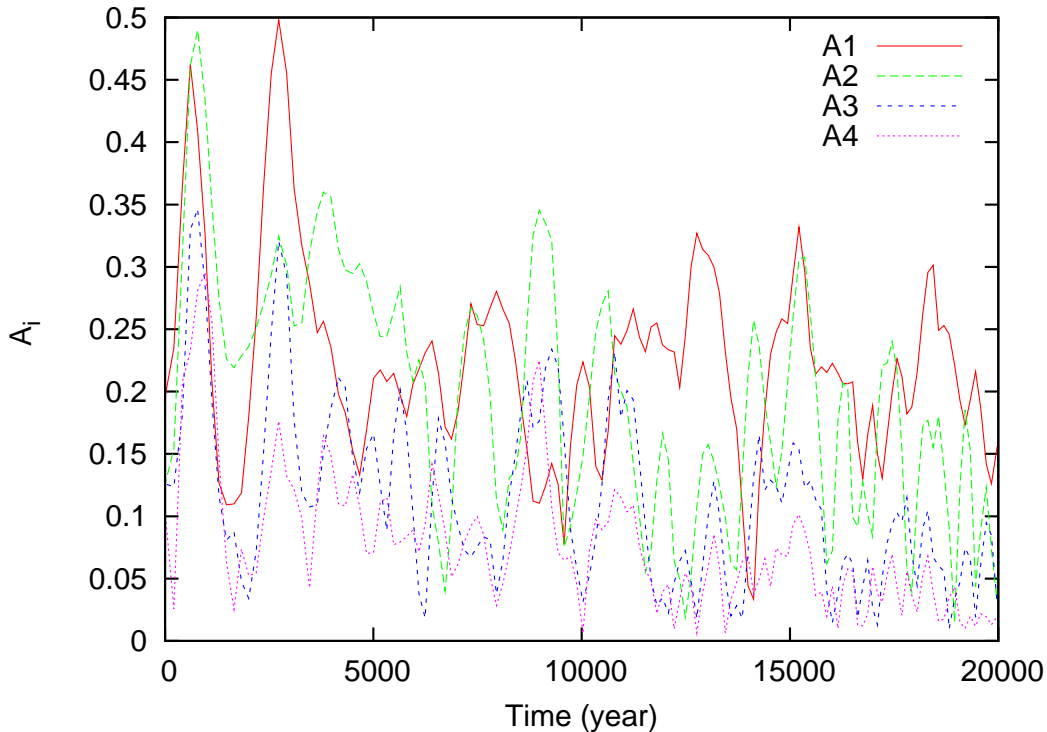


**Figure 3.** Evolution of Fourier amplitudes of surface density at 100 AU against elapsed time after protostar formation for model 4.

As shown in Figure 1, the structure of the disk is highly non-axisymmetric, which is caused by non-axisymmetric accretion from large-scale filaments. To clarify this, we plot in Figure 3 the Fourier amplitudes of the surface density at 100 AU for  $2.0 \times 10^4$  years after protostar formation. The Fourier amplitudes are calculated from a Fourier series,

$$\frac{\Sigma(R, \phi)}{\bar{\Sigma}(R)} = \sum_{m=1}^{\infty} A_m \exp[-im\phi], \quad (7)$$

where  $m$  is the azimuthal wavenumber and  $A_m$  is the Fourier amplitude. Figure 3 shows that most of the time, the  $m = 1$  mode dominates the other modes, although the  $m = 2$  mode occasionally dominates the  $m = 1$  mode. In addition, the amplitude of other higher modes ( $m \geq 3$ ) is smaller than that of modes  $m = 1$  and 2. The prominent  $m = 1$  mode is a significant feature of disks with non-axisymmetric envelope accretion.

Figure 4 shows the time evolution of an edge-on view of the center of the cloud core for model 4. The figure indicates that the disk orientation varies during main accretion phase. We discuss the evolution of the disk orientation further in §3.2.

As we showed above, the evolution process of a circumstellar disk in a strong turbulent core is different from that in a rapidly rotating core in many respects. As we will see below, the evolution process becomes similar to that of a rigidly rotating cloud core as the turbulent energy decreases. However, note that the dynamical change of the disk orientation also occurs even in the weak turbulent core.

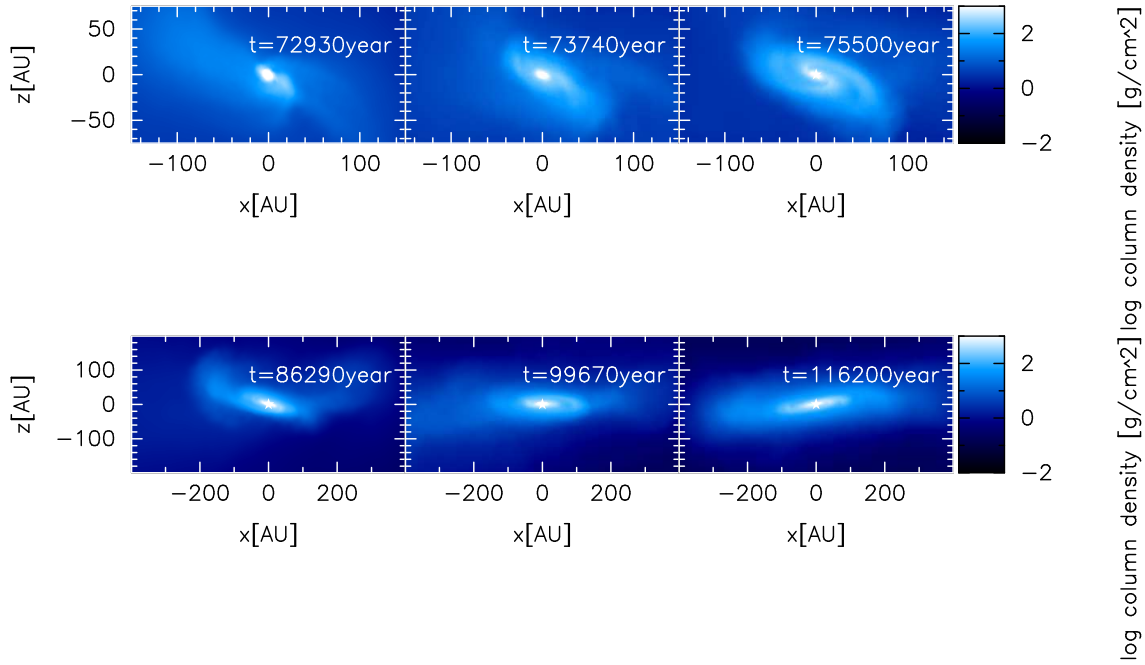
### 3.1.2 Disk evolution in weak turbulent core

As a typical case for the formation and evolution of a circumstellar disk in a weakly turbulent cloud core, we chose model 6 that has parameters of  $\alpha = 0.4$  and  $\gamma_{\text{turb}} = 0.06$ . The initial rms Mach number is 0.63. Compared with model 4 (strong turbulent case), model 6 has the same thermal energy but a smaller turbulent energy.

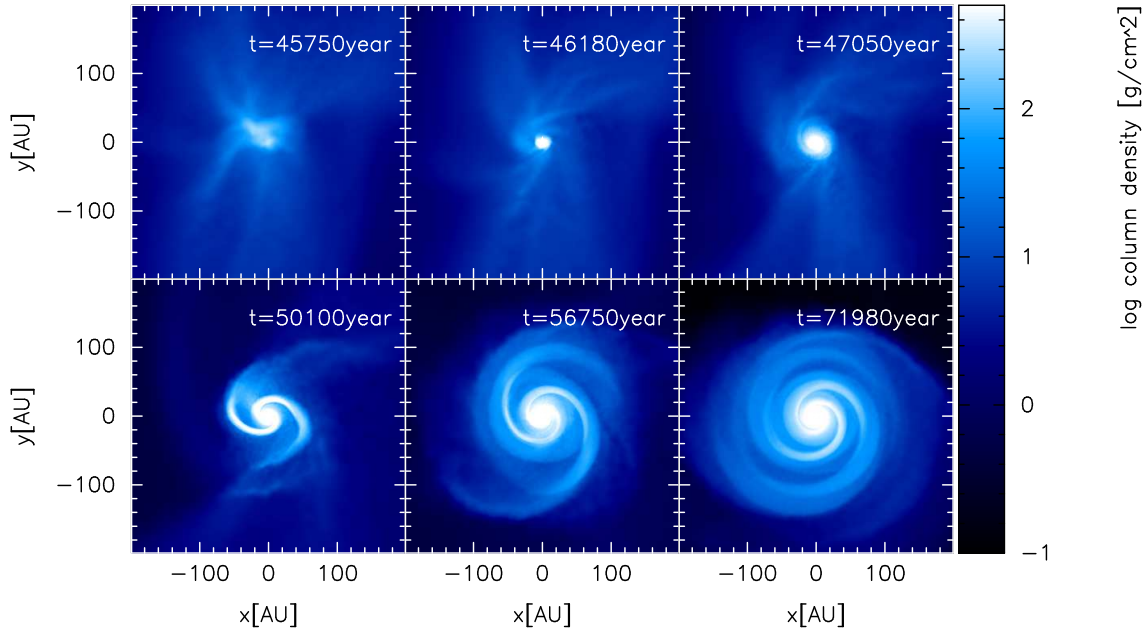
Figure 5 shows a face-on view of the time evolution of the center of the cloud core. Before protostar formation (top-left panel), some filaments appear and form a complicated structure. However, the density amplitude of filaments appearing in this model is much weaker than what appears in the models which initially have strong turbulence. As the mass accretion onto disk proceeds, the circumstellar disk becomes massive and develops the spiral arms (bottom panels). Finally, the radius of the circumstellar disk reaches  $\gtrsim 100$  AU. The filaments that appear in the early evolution phase (top panels) are attributed to anisotropic gas accretion in a weakly turbulent environment, whereas the spirals that appear in the later evolution phase (bottom panels) develop because of gravitational instability of the disk itself.

Figure 6 shows the disk evolution when viewed edge-on. The results indicate that the disk orientation varies with time even with the weak turbulence. As we will see in §3.2, the dynamical change of the disk orientation generally occurs independent of the strength of the turbulence. The fluctuation of the disk orientation is a significant feature of disk evolution in turbulent cloud cores.

Figure 7 shows the radial profiles of the surface density (top) and radial velocity (bottom) for model 6; the solid, dashed, dotted, and dashed-dotted lines correspond to the top-middle, bottom-left, bottom-middle, and bottom-right



**Figure 4.** Same as Figure 1 but edge-on view.



**Figure 5.** Time sequence of logarithm of face-on surface density before and after protostar formation for model 6 ( $\alpha = 0.4$  and  $\gamma_{\text{turb}} = 0.06$ ). The  $z$ -axis is parallel to the angular momentum of the entire initial cloud core. Top-left panel shows a snapshot approximately  $4.3 \times 10^2$  years before protostar formation. Top-middle panel shows a snapshot just when the protostar forms. Top-right, bottom-left, -middle, and -right show snapshots  $8.7 \times 10^2$  years,  $3.9 \times 10^3$  years,  $1.1 \times 10^4$  years, and  $2.6 \times 10^4$  years after protostar formation, respectively. The elapsed time in the calculation is shown in each panel.

panels in Figure 5, respectively. The top panel of Figure 7 shows that the disk gradually increases in size and surface density with time. In addition, the figure shows that a disk-like structure of size  $\sim 10$  AU already exists before and immediately after protostar formation (solid line). This indicates that the remnant of the first core changes directly into

the circumstellar disk. Thus, the formation and evolution processes of the circumstellar disk in weakly turbulent cloud cores are qualitatively the same as those in slowly and rigidly rotating cloud cores seen in previous works (see, e.g., Bate 2011; Machida et al. 2010). In the bottom panel of Figure 7, a positive radial velocity arises in the range of 50–100 AU

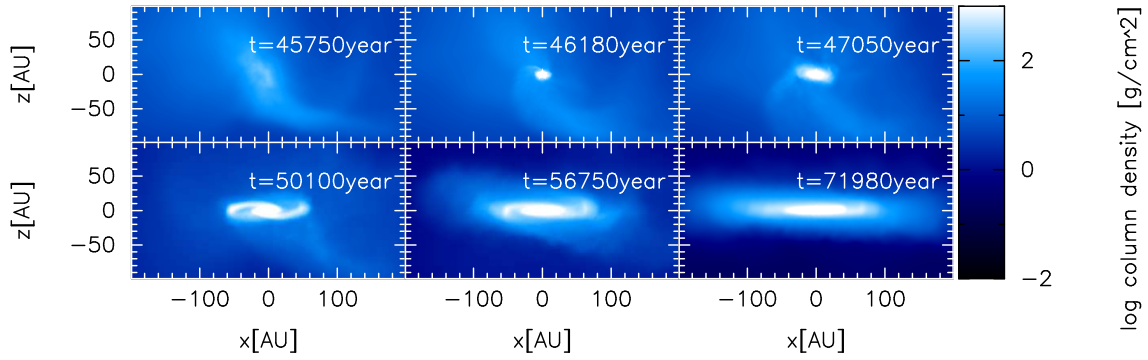


**Figure 6.** Same as Figure 5 but edge-on view.

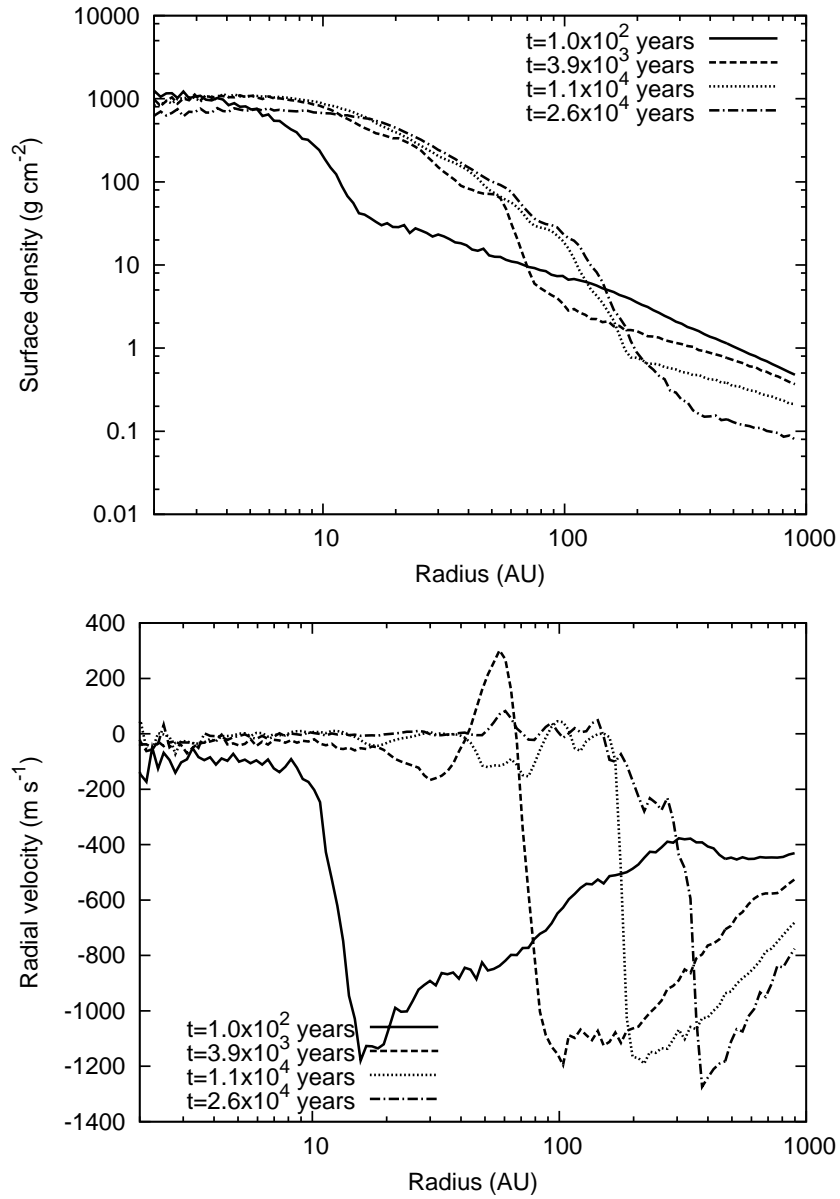


**Figure 7.** Radial distribution of surface density (top) and radial velocity (bottom) for model 6. Lines corresponds to  $1.0 \times 10^2$  years (solid),  $3.9 \times 10^3$  years (dashed),  $1.1 \times 10^4$  years (dotted), and  $2.6 \times 10^4$  (dashed-dotted) years after protostar formation.



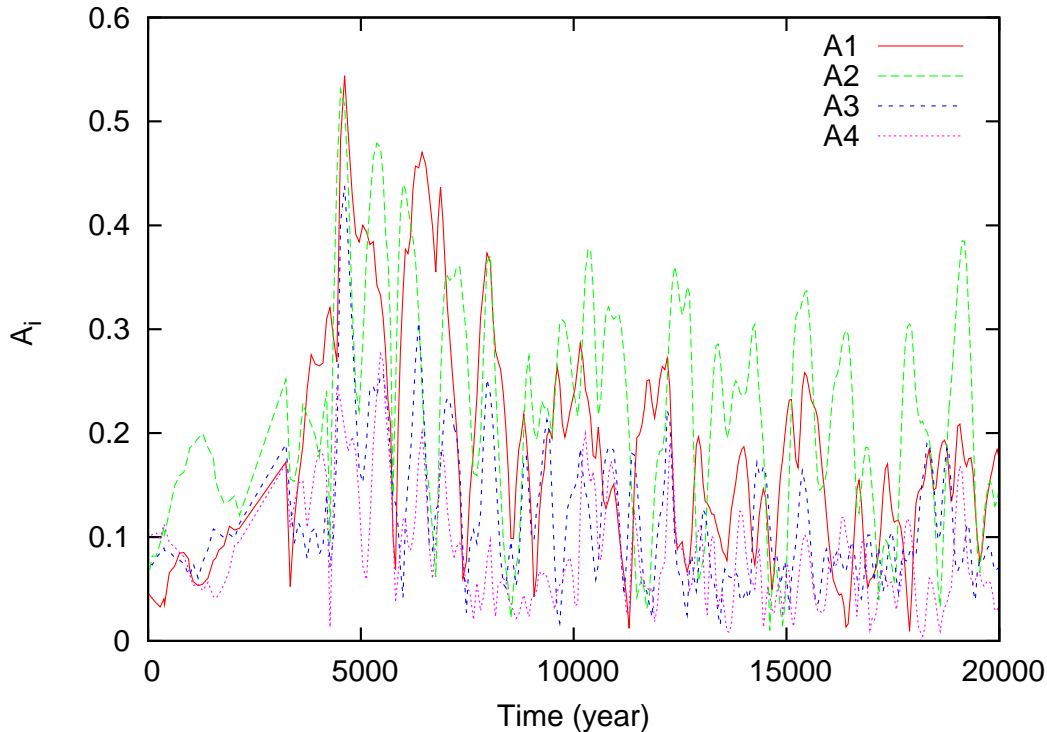


**Figure 8.** Evolution of Fourier amplitudes of surface density at 100 AU versus elapsed time after protostar formation for model 6.

at  $\sim 5.0 \times 10^3$  years after the second collapse. This outward flow in the disk is due to the  $m = 2$  mode of spiral arms.

Figure 8 shows the Fourier amplitudes of the surface density at 100 AU for  $2 \times 10^4$  years after protostar formation for model 6. For  $t \lesssim 5 \times 10^3$  years, the disk radius is smaller than 100 AU. Thus, these amplitudes during this epoch originate not from the circumstellar disk but from anisotropic accretion from the infalling envelope. After the circumstellar disk grows sufficiently, unlike the model which have strong turbulence, the  $m = 2$  mode dominates the other modes, especially for  $t \gtrsim 1 \times 10^3$  years, as shown in the bottom-right panel of Figure 6.

As seen in previous studies (Laughlin et al. 1998; Lodato & Rice 2005), without gas accretion onto the disk, the gravitational instability of the disk tends to develop the  $m = 2$  spiral arms. Because of the weak turbulence in this model, the gas falls almost isotropically onto the circumstellar disk. Thus, the prominence of the  $m = 2$  mode is attributed to the gravitational instability of the disk. On the other hand, the model with the strong turbulence, the  $m = 1$  density perturbation mode is dominant in the disk. This  $m = 1$  mode is considered to be caused by anisotropic gas accretion onto the circumstellar disk. Note that the initial density perturbation of the disk strongly affects the non-linear development of the spiral arms (Laughlin & Bodenheimer 1994). These major modes play an important role in angular momentum transfer and readjust the surface density toward a more stable configuration.

### 3.2 Evolution of Disk Orientation

Figure 9 shows the time evolution of the angle of orientation of the disk angular momentum with respect to the angular momentum of the entire initial cloud core for non-fragmentation models (models 1–6). Because the disk is mainly supported by rotation, the orientation of the disk angular momentum roughly corresponds to the disk orientation. The disk angular momentum (disk orientation) is parallel to the angular momentum of the initial cloud core when  $\theta = 0$ . In the figure, the origin of time is set to the epoch when the protostar forms. This figure shows that the disk orientation is generally misaligned with respect to the total angular momentum of its host core at its formation and dynamically changes during the main accretion phase regardless of the strength of the turbulence. In each model, the angle of orientation of the disk is  $30^\circ$ – $60^\circ$  toward the angular momentum of the initial cloud core at the protostar-formation epoch ( $t = 0$ ). As the accretion proceeds, the angle of orientation gradually decreases, reaching  $\theta \lesssim 15^\circ$  within several  $10^4$  years for all models. It is expected that the disk orientation will be aligned with the angular momentum of the cloud core when the gas accretion ceases.

The right panel of Figure 9 shows that the angle of orientation for model 2 ( $\alpha = 0.6$  and  $\gamma_{\text{turb}} = 0.06$ ) varies irregularly with time. In the model, a very compact disk ( $\lesssim 10$  AU) forms at first. It accretes onto the protostar and disappears in a short duration of  $\sim 10^3$  years. Then, another larger disk forms by the subsequent mass accretion. Reflecting this disk disappearance, model 2 shows an irregular evolution of disk orientation. This irregular evolution in the early disk evolution stage may be unrealistic because of artificial treatment of the accretion onto the sink parti-

cle. However, this treatment for sink particle does not qualitatively change our claim that the disk orientation angle dynamically changes with time.

### 3.3 Fragmentation and Evolution of Disks in Binary System

In models 7–9, fragmentation of filament occurs and a binary or multiple stellar system appears, whereas only a single protostar forms in models 1–6. The fragmentation process in a turbulent cloud core differs considerably from that in a cloud core with initial rigid rotation. Figure 10 shows the density distribution when the protostars form for models 7–9. The figure indicates that the binary or multiple system forms by fragmentation of the filament. The figure also shows that the disks in a binary or multiple systems are not aligned with each other. For these fragmentation models, fragmentation tends to occur near the edge of the filament. This fragmentation process is possible to be explained by the focal point scenario suggested by Burkert & Hartmann (2004).

To investigate further evolution of a wide binary system and disk evolutions, we focus on model 7 ( $\alpha = 0.2$  and  $\gamma_{\text{turb}} = 0.3$ ). Figure 11 shows the time evolution of the binary separation and its orbital energy for model 7. The orbital energy is given as

$$E_{\text{orbit}} = \frac{1}{2}v^2 - \frac{G(m_1 + m_2)}{r}, \quad (8)$$

where  $r$  and  $v$  are the relative distance and relative velocity, respectively. Note that the mass of protostar changes during the simulation. **The right panel shows that the orbital energy steadily decreases, indicating that the binary system loses its orbital energy by tidal interaction between the disks and stars. In the left panel, we can see the separation of the binary also decreases.** Therefore, it is expected that the observed separation of a binary or multiple system does not reflect the initial separation. **In the right panel, sharp increases of the orbital energy are caused by the close encounter. During the early phase of binary formation, each disk is more massive than its host star and the stars are also accelerated by their surrounding disks. In equation (8), since the kinetic and potential energies of the disks are not included, this orbital energy is not conserved. Therefore, the orbital energy shows a large fluctuation at every close encounter. Note that it is considerably difficult to estimate the orbital energy of whole system which consider the stars and disks, because the disks exchange their mass and a part of the disk gas is striped off when close encounter occurs. However, we can roughly understand the evolution of the separation and the orbital energy of the binary system for a long duration with Figure 11. Note also that, the binary stars sometime have a positive orbital energy, which seems to indicate that the binary system is not gravitationally bounded. However, the sign of orbital energy has no meaning since we ignored the disk component in equation (8). We confirmed that the whole system (disks and stars) are gravitationally bounded during this epoch.**

Figure 12 shows an edge-on snapshot around the binary system at the end of the simulation ( $t = 2.5 \times 10^4$  years

after the second protostar formation). Because the disk orientation around each protostar is mainly determined by the local velocity field at which the protostar forms, the disks are not aligned with each other. The misalignment is also seen in model 8. Thus, it seems that the misalignment between disks is general feature of binary/multiple systems which form via filament fragmentation and initially have large separation ( $\gtrsim 100$  AU).

The left panel of Figure 13 shows the evolution of the orientation angle of the disks from the angular momentum direction of the host core and the mutual inclination between the primary and secondary disks. In this study, we call the circumstellar disk around the primary protostar the primary disk and that around the secondary protostar the secondary disk. The angle of the primary disk orientation is  $\sim 90^\circ$  in the very early phase of disk formation and it decreases with time (right panel). The sudden increases at  $t = 6 \times 10^3$ ,  $1.6 \times 10^4$ , and  $2.4 \times 10^4$  years are due to close encounters, as seen in Figure 11. At each close encounter, the angle variation for the secondary disk is larger than that for the primary disk, which is because of the secondary disk is less massive than the primary disk. Thus, the secondary disk is strongly affected by the tidal interaction. As seen in the right panel of Figure 13, the primary and secondary disks are inclined from the orbital plane by approximately  $50^\circ$  and  $30^\circ$  at the end of the simulations.

## 4 DISCUSSION

### 4.1 Dynamical Change of Disk Orientation

As shown in Figure 9, the disk orientation is generally misaligned with the angular momentum of its host cloud core and dynamically changes during the main accretion phase even in a weakly turbulent cloud. This is because the angular momentum of the entire cloud core is determined mainly by the velocity field, whose wavelength is comparable to the cloud scale,  $\lambda \sim R_{\text{cloud}}$ . On the other hand, the angular momentum of the disk is determined by the local velocity field, whose wavelength is much smaller than the cloud size,  $\lambda \ll R_{\text{cloud}}$ . There is no phase correlation between these scales. This nature is independent of the strength of turbulence. The disk orientation changes due to the mass accretion which brings the angular momentum. The variation in the disk orientation during the main accretion phase can explain the precessing outflow (e.g., Cunningham et al. 2009) because the outflow is believed to be driven by the circumstellar disk.

### 4.2 Misaligned Disks in Binary Systems

When large-scale fragmentation occurs and the binary system initially has a wide separation, disks tend to be misaligned because there is no correlation between the velocity fields in different regions. Thus, when a wide binary system forms in a turbulent cloud core, disks are expected to be misaligned with each other and also misaligned with the binary orbital plane at their formation epoch. Our simulation showed that the misalignment can maintain at least for several  $10^4$  years. Roccatagliata et al. (2011) recently observed a proto-binary system embedded in a common envelope and

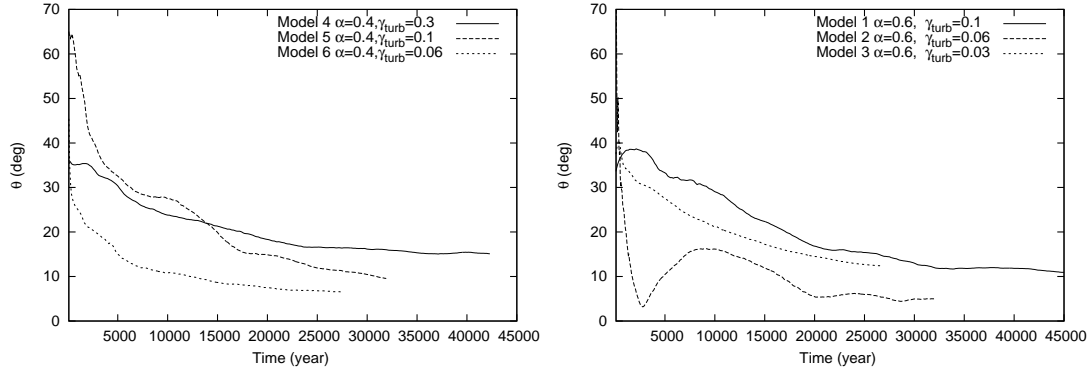


**Figure 9.** Time evolution of orientation of disk angular momentum. The orientation angle  $\theta = 0$  corresponds to the orientation of the angular momentum of the initial cloud core. Left panel shows models having  $\alpha = 0.4$ , in which the solid, dashed, and dotted lines correspond to models with parameters of  $\gamma_{\text{turb}} = 0.3, 0.1$ , and  $0.06$ , respectively. Right panel shows models having  $\alpha = 0.6$ , in which the solid, dashed, and dotted lines correspond to models with  $\gamma_{\text{turb}} = 0.1, 0.06$ , and  $0.03$ , respectively.

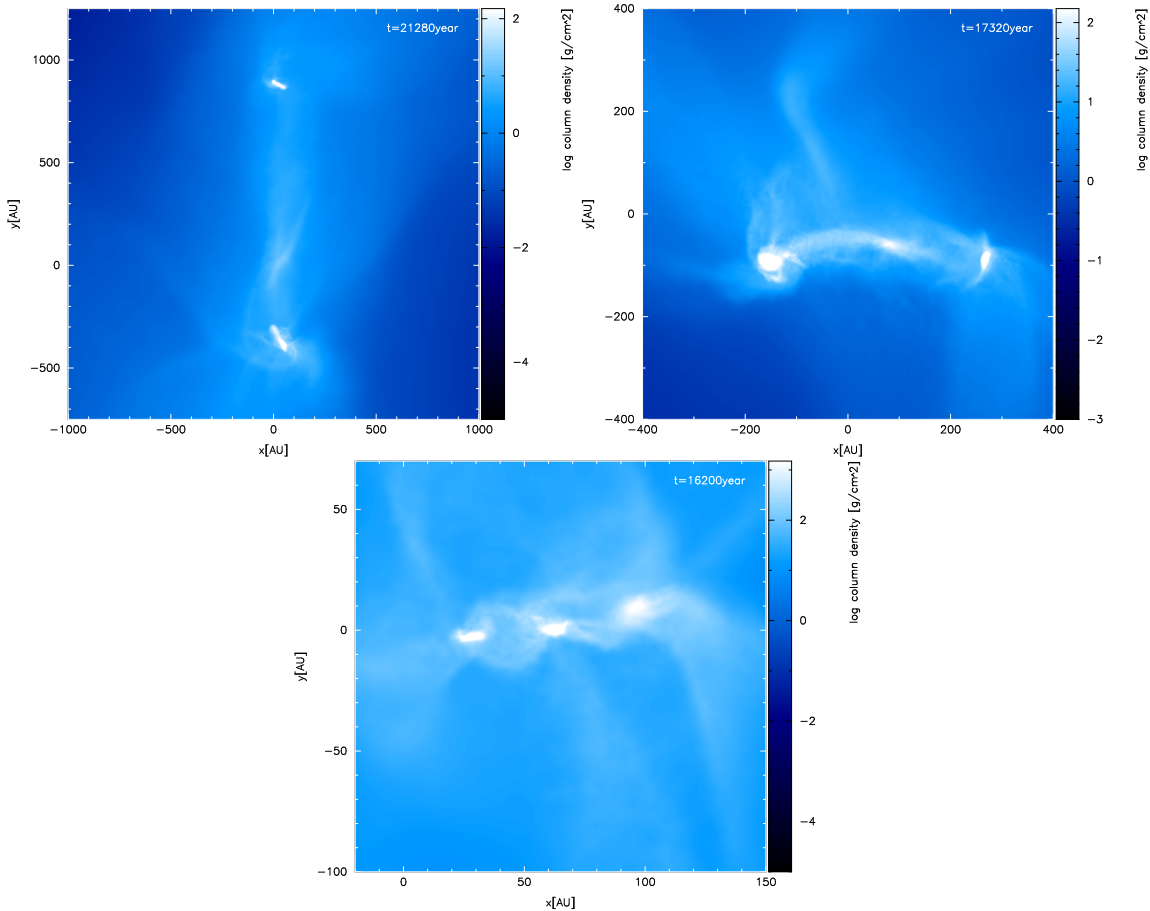


**Figure 10.** Logarithm of face-on surface density when a binary or multiple system appears in models 7 (top left,  $\gamma_{\text{turb}} = 0.3$ ), 8 (top right,  $\gamma_{\text{turb}} = 0.1$ ) and 9 (bottom,  $\gamma_{\text{turb}} = 0.06$ ). Models 7–9 have the same initial thermal energy of  $\alpha = 0.2$ .

showed that the disks are highly misaligned (edge-on and face-on disks). They suggested that such a binary system is formed by fragmentation of two different parts of the collapsing molecular cloud core. Our study can naturally explain such misaligned disks in a binary system. Misaligned disks are also observed even in a multiple stellar system (Ratzka et al. 2009). Our result also indicates that such a

system can form via fragmentation of the collapsing cloud core in a turbulent environment, as seen in Figure 10.

We can also expect the disk orientation in a binary system from observations of molecular outflows or optical jets. Chen et al. (2008) observed a low-mass protostellar binary system and discovered two high-velocity bipolar molecular outflows that were nearly perpendicular to each other,

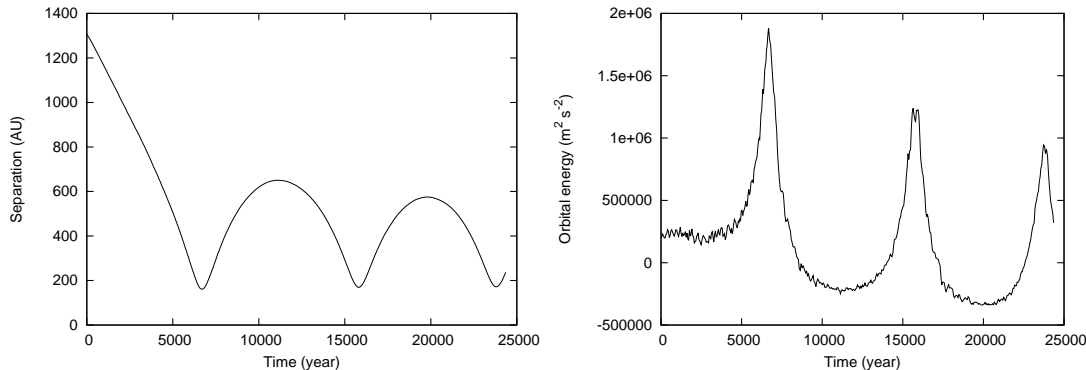


**Figure 11.** Time evolution of the separation between primary and secondary protostars (left) and the orbital energy (right) for model 7.

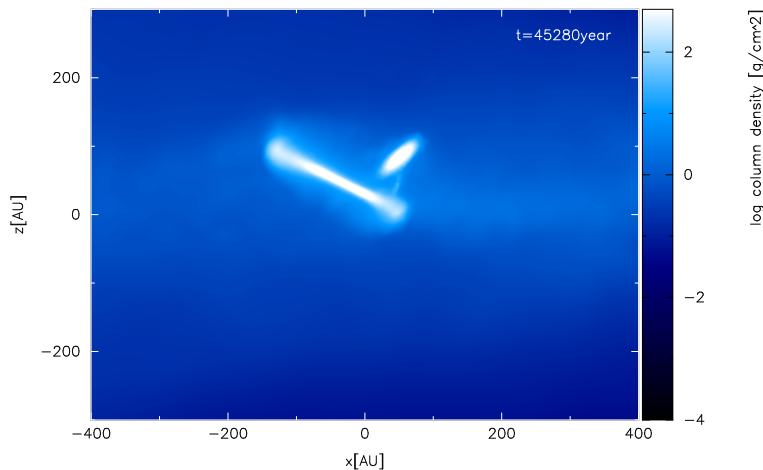


**Figure 12.** Surface density distribution at end of calculation for model 7 ( $\alpha = 0.2$  and  $\gamma_{\text{turb}} = 0.3$ ). Calculation stops  $2.5 \times 10^4$  years after the secondary protostar forms.

showing a quadruple morphology. They concluded that the disks in a wide binary system are not necessarily co-aligned after fragmentation. A quadrupolar morphology and misaligned outflows are often observed in young binary systems (Mizuno et al. 1990; Gueth et al. 2001; Lee et al. 2002; Carrasco-González et al. 2008). Because outflows or jets are expected to be driven by the disk, misaligned disks are expected to show misaligned outflows. Therefore, observations of wide binary systems and our results support the idea that a binary/multiple system forms via dynamical fragmentation of the filament in a turbulent molecular cloud core.

### 4.3 Further Disk Evolution and Implications for Planet Formation in Binary System

Tidal interaction between disks and protostars in binary system is essential for further evolution of disk orientation in binary system. Papaloizou & Terquem (1995) showed that perturbation of the secondary star can align the primary disk toward the binary orbital plane. Bate et al. (2000) also showed that the disk can be aligned with the binary orbital plane on the precession time-scale owing to tidal interaction. Thus, whether the disk is aligned with the orbital plane depends on the parameters of the binary system (especially

on the orbital period). On the other hand, observations of main-sequence binary systems indicate that the stellar rotational equatorial planes (which may reflect the orientations of the disks) in wide binary systems ( $\gtrsim 40$  AU) are often misaligned with the binary orbital plane (Hale 1994). Thus, in wide binary system, disk misalignment is often maintained even after the main accretion phase.

When disk misalignment remains after the main accretion phase, it is important for planet formation and the orbital evolution of planets in a binary system. When planet formation in a binary system is investigated, it is conventionally assumed that each disk is aligned with the binary orbital plane (Marzari & Scholl 2000; Tsukamoto & Makino 2007). However, when the disk and the binary orbital plane are mutually misaligned, the planet formation processes drastically change. By the Kozai effect (Kozai 1962), inward migration of planetesimals occurs. Thus, a compact dense planetesimal disk forms (Xie et al. 2011). On the other hand, the Kozai migration mechanism (Fabrycky & Tremaine 2007) seems to be preferable for explaining the existence of close-in planets if disk misalignment generally occurs. Narita et al. (2010) recently found that the orbital plane of the planets is generally not aligned with the orbital plane of the binary system. This also seems to be explained by the idea that the disks

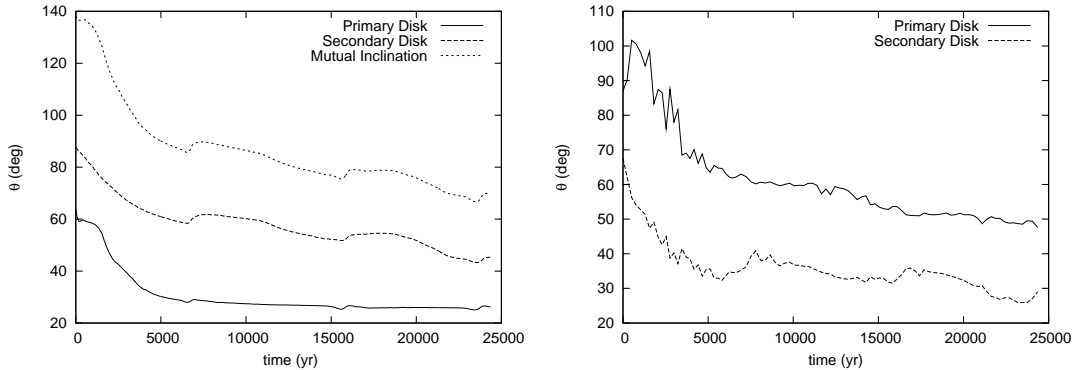


**Figure 13.** Left panel shows time evolution of angle of disk orientation with respect to angular momentum of initial cloud core for primary (solid line) and secondary (dashed line) disks, and mutual inclination between the primary and secondary disks (dotted line). Right panel shows the time evolution of the inclination of the primary (solid line) and secondary (dashed line) disks toward the binary orbital plane.

were misaligned with the binary orbital plane during the formation epoch.

#### 4.4 Comparison with Disk Evolution Simulations in Turbulent Cloud Core

Goodwin et al. (2004a,b) investigated the evolution of turbulent cloud cores. As we mentioned in §2.2.2, they considered an ensemble of simulations with different random number seeds, and showed that fragmentation frequently occurs even with a moderate accretion rate that is realized in cloud cores with initially weak turbulence ( $\alpha = 0.45$  and  $\gamma_{\text{turb}} = 0.05$ ). Their results are qualitatively the same as ours: fragmentation occurs in turbulent cloud cores and turbulence promotes fragmentation. However, the fragmentation condition shown in Goodwin et al. (2004a,b) seems to be quantitatively different from ours, because fragmentation only occurs with high accretion rate ( $\alpha \leq 0.2$  and  $\gamma_{\text{turb}} > 0.06$ ) in our simulations. This difference may originate in the difference of initial conditions. In their study, the initial cloud cores with a Plummer-like density profile has a total mass of  $M = 5.4M_{\odot}$ . On the other hand, in our study, the initial cloud cores with a uniform density profile has a total mass of  $M = 1M_{\odot}$ . Thus, although it is difficult to quantitatively compare our results with Goodwin et al. (2004a,b), the difference in initial conditions may somewhat changes the fragmentation condition. It is also possible that the different numerical resolutions may also affect the fragmentation condition. They resolved the cloud core with 25000 particles, whereas we resolved it with 520000 particles. Mass resolutions in their study and in our study are  $m_{\text{res}} = 2.1 \times 10^{-4}$  and  $1.9 \times 10^{-6} M_{\odot}$ , respectively, which implies that spatial resolution in our simulation is approximately five times higher than in theirs. As discussed in Nelson (2006), there is a possibility that the lower spatial resolution may enhance disk fragmentation.

Walch et al. (2010) investigated the evolution of turbulent cloud cores whose mass is  $M_{\text{core}} = 6.1M_{\odot}$ . They fixed the mean Mach number of cloud cores to be  $\mathcal{M} = 1$  and changed the minimum and maximum turbulent wavelength and random seeds. In their study, the sum of the thermal and kinetic energies exceeds the gravitational energy, (i.e.,

$\alpha + \gamma_{\text{turb}} > 1$ ). Thus, initial cloud cores are gravitationally unbound as a whole. The cloud begins to collapse after the energy dissipates by radiative cooling. By this approach, the consistency of the density distribution and the velocity field can be realized before the collapse begins. But it is difficult to control the accretion rate onto the disk with simple parameters. Note that, in our study, the accretion rate can be controlled by the parameters  $\alpha$  and  $\gamma_{\text{turb}}$  because we adopted cloud cores that were initially gravitationally unstable. They pointed out that initial differences of the angular momentum rarely affects the evolution of the cloud and circumstellar disk. Rather, a filamentary structure appearing in turbulent cloud cores affects the evolution of the protostar and disk. Their results seem to be in agreement with ours. However, whereas a clear spiral arm often develops after disk formation in our simulation, most of the disks formed in their simulations does not develop the spiral arms. This difference may come from difference in the accretion rate.

The evolution of low-mass very cold cores with a cloud mass of  $M_{\text{core}} = 1.28 M_{\odot}$  was investigated in Walch et al. (2012). They focused on the relationship between the evolution of the core and the maximum wavelength of the turbulence. They pointed out that the dynamical fragmentation of filaments is a major process for binary formation in turbulent cloud cores. They demonstrated that binary formation via disk fragmentation is rare in the early phase of protostar formation which seems to be in agreement with our results. Their initial conditions are very cold and turbulence is very weak. Thus, disks formed in their simulations are very compact compared with ours (see, Fig. 1 or 5 and Fig. 2 of Walch et al. 2012). In this study, we focused on the relationship between the evolution of the circumstellar disk and the turbulent energy of the cloud core. Furthermore, we showed how the disk orientation varies in time which is not mentioned in their study.

#### 4.5 Validity of Initial Conditions

##### 4.5.1 Inconsistency between the velocity and density field and possible effects on the results

As described in §2, we imposed the turbulent velocity field (Gaussian random field) on the uniform density field. Thus,

they are not self-consistent when the simulation begins. Thus, it is expected that the velocity field do work to establish self-consistent density field during the early phase of cloud evolution and the turbulence would decay. This decay could change the effective turbulent energy for the simulations. Another possible effect is that the density field could be still inconsistent even after the disk formation because our initial conditions are gravitationally bounded ( $\alpha + \gamma_{\text{turb}} < 1$ ) and gravitational collapse immediately begins. In this subsection, we discuss whether these effects change our results.

In figure 14, to investigate how much the turbulence decay, we show the time evolution of the velocity dispersion in the isothermal phase (maximum density of cloud is less than the critical density,  $\rho_{\text{max}} < \rho_c$ ) for model 4 as an example. In the figure, the velocity dispersion slightly decreases due to the loss of turbulence energy for  $t \lesssim 60000$  years. Then, it turns to increase at  $t \sim 60000$  years, and continues to increase for  $t \gtrsim 60000$  years. This increase is attributed to the infall motion of the cloud. This figure indicates that the decrease of turbulent energy before the cloud collapse is not so large. Thus, it is expected that this energy loss rarely affects the subsequent cloud evolution significantly. We confirmed that the turbulent energy loss in other models is also small.

Next, we discuss how the inconsistent density field affects the evolution of the system. In this study, we showed (i) anisotropic accretion enhances the low-order mode of spiral arms in the disk, (ii) the disk orientation dynamically changes during the main accretion phase, and (iii) the orientation of the disks is mutually misaligned and also misaligned with the orbital plane in binary system if the binary stars form in different region (or initial separation is sufficiently large). They are all originated from the anisotropic gas accretion onto the disk. The inconsistent density field would be smoother than a more realistic (or self-consistent) density field. Thus, if the self-consistent density field is adopted for the initial conditions, it is expected that the anisotropic accretion may be enhanced. Thus, all the above features should be more stressed but not suppressed. Therefore, our results are not changed by the inconsistent density field.

#### 4.5.2 *Validity of High Mach Number or Highly Gravitationally Unstable Initial Conditions*

In this study, to comprehensively understand the relation between turbulence and disk evolution, we adopted over a wide range of parameters and investigated both the disk formation around single star and in binary system. To investigate the disk evolution process around the binary system, we adopted a bit artificial initial conditions: initial cloud core of model 7 has large Mach number ( $\mathcal{M} > 1$ ) which is much larger than the typical observed value in cloud cores with masses of order 1 Msolar, and cores of models 8 and 9 are in highly gravitationally unstable state ( $\alpha + \gamma_{\text{turb}} = 0.3$  and 0.26). If our results and conclusions are closely related to the artificial aspects of these initial conditions, it is problematic.

However, we would like to emphasize that our finding is not related to it. The main results we obtained from the simulations of model 7, 8 and 9 are that the disk orientation of binary system generally misaligned each other and from or-

bit plane if the initial separation of protostars is sufficiently large. This is because there is no correlation between the local velocity fields where the protostars forms. It is fundamental property of turbulence that there is no correlation between the local velocity fields around the different positions. Thus, such a misalignment may occur in the actual molecular cloud core in which binary system forms. This should be confirmed by the observation and we think the observations we mentioned above (Hale 1994; Roccatagliata et al. 2011) seem to support our results.

## ACKNOWLEDGMENTS

We thank S. Inutsuka, T. Tsuribe, K. Osuga, K. Tomisaka, S. Okuzumi, and K. Tomida for the fruitful discussions. We also thank the anonymous referee for valuable comments. The snapshots were produced by SPLASH (Price & Monaghan 2007). The computations were performed on a parallel computer, the XT4 system at CfCA of NAOJ and SR16000 at YITP in Kyoto University. Y.T. is financially supported by Research Fellowships for Young Scientists from JSPS.

## REFERENCES

- Balsara, D. S. 1995, *Journal of Computational Physics*, 121, 357
- Bate, M. R. 1998, *ApJ*, 508, L95
- . 2011, *MNRAS*, 417, 2036
- Bate, M. R., Bonnell, I. A., Clarke, C. J., Lubow, S. H., Ogilvie, G. I., Pringle, J. E., & Tout, C. A. 2000, *MNRAS*, 317, 773
- Bate, M. R., Bonnell, I. A., & Price, N. M. 1995, *MNRAS*, 277, 362
- Bate, M. R. & Burkert, A. 1997, *MNRAS*, 288, 1060
- Burkert, A. & Bodenheimer, P. 2000, *ApJ*, 543, 822
- Burkert, A. & Hartmann, L. 2004, *ApJ*, 616, 288
- Carrasco-González, C., Anglada, G., Rodríguez, L. F., Torrelles, J. M., Osorio, M., & Girart, J. M. 2008, *ApJ*, 676, 1073
- Chen, X., Bourke, T. L., Launhardt, R., & Henning, T. 2008, *ApJ*, 686, L107
- Cunningham, N. J., Moeckel, N., & Bally, J. 2009, *ApJ*, 692, 943
- Davis, C. J., Mundt, R., & Eisloffel, J. 1994, *ApJ*, 437, L55
- Dubinski, J., Narayan, R., & Phillips, T. G. 1995, *ApJ*, 448, 226
- Fabrycky, D. & Tremaine, S. 2007, *ApJ*, 669, 1298
- Goodman, A. A., Benson, P. J., Fuller, G. A., & Myers, P. C. 1993, *ApJ*, 406, 528
- Goodwin, S. P., Whitworth, A. P., & Ward-Thompson, D. 2004a, *A&A*, 414, 633
- . 2004b, *A&A*, 423, 169
- Gueth, F., Schilke, P., & McCaughrean, M. J. 2001, *A&A*, 375, 1018
- Hale, A. 1994, *AJ*, 107, 306
- Inutsuka, S.-i., Machida, M. N., & Matsumoto, T. 2010, *ApJ*, 718, L58
- Klessen, R. S. 2000, *ApJ*, 535, 869

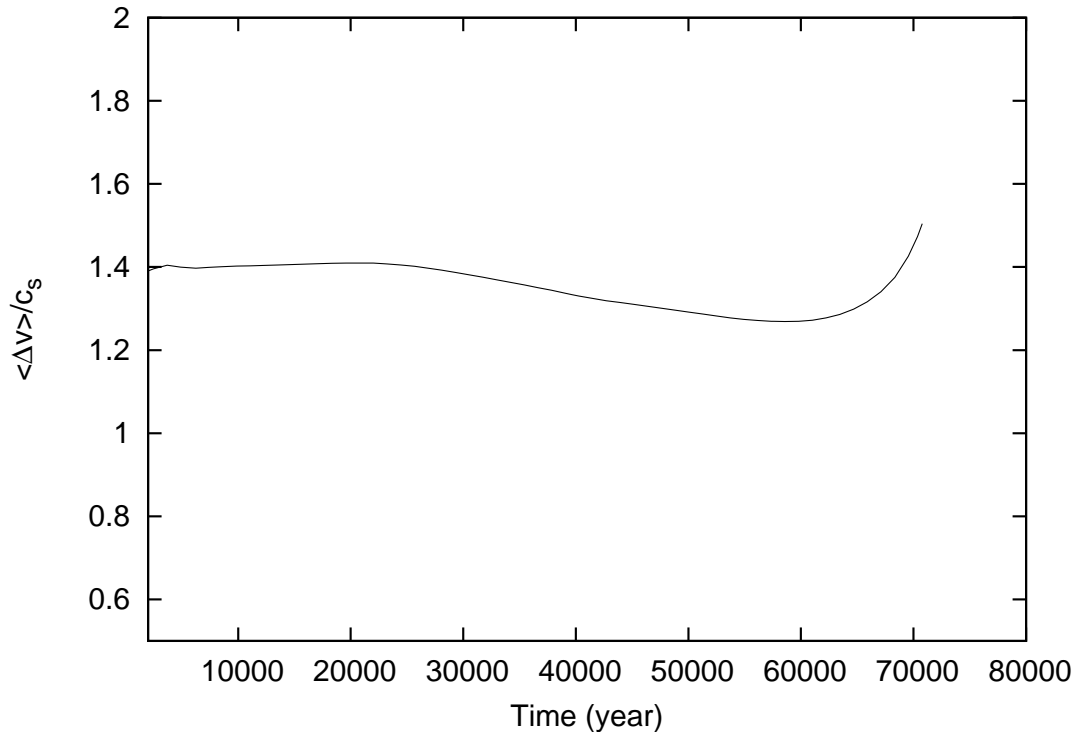


**Figure 14.** Velocity dispersion,  $\Delta v$  as a function of time in the isothermal collapse phase is shown.

- Kozai, Y. 1962, *AJ*, 67, 591
- Larson, R. B. 1969, *MNRAS*, 145, 271
- Laughlin, G. & Bodenheimer, P. 1994, *ApJ*, 436, 335
- Laughlin, G., Korchagin, V., & Adams, F. C. 1998, *ApJ*, 504, 945
- Lee, C.-F., Mundy, L. G., Stone, J. M., & Ostriker, E. C. 2002, *ApJ*, 576, 294
- Lodato, G. & Rice, W. K. M. 2005, *MNRAS*, 358, 1489
- Machida, M. N., Inutsuka, S.-i., & Matsumoto, T. 2010, *ApJ*, 724, 1006
- Machida, M. N. & Matsumoto, T. 2011, *MNRAS*, 413, 2767
- Marzari, F. & Scholl, H. 2000, *ApJ*, 543, 328
- Masunaga, H. & Inutsuka, S.-i. 2000, *ApJ*, 531, 350
- Matsumoto, T. & Hanawa, T. 2011, *ApJ*, 728, 47
- Miyama, S. M., Hayashi, C., & Narita, S. 1984, *ApJ*, 279, 621
- Mizuno, A., Fukui, Y., Iwata, T., Nozawa, S., & Takano, T. 1990, *ApJ*, 356, 184
- Monaghan, J. J. 1997, *Journal of Computational Physics*, 136, 298
- Narita, N., Kudo, T., Bergfors, C., Nagasawa, M., Thalmann, C., Sato, B., Suzuki, R., Kandori, R., Janson, M., Goto, M., Brandner, W., Ida, S., Abe, L., Carson, J., Egner, S. E., Feldt, M., Golota, T., Guyon, O., Hashimoto, J., Hayano, Y., Hayashi, M., Hayashi, S. S., Henning, T., Hodapp, K. W., Ishii, M., Knapp, G. R., Kusakabe, N., Kuzuhara, M., Matsuo, T., McElwain, M. W., Miyama, S. M., Morino, J.-I., Moro-Martin, A., Nishimura, T., Pyo, T.-S., Serabyn, E., Suenaga, T., Suto, H., Takahashi, Y. H., Takami, M., Takato, N., Terada, H., Tomono, D., Turner, E. L., Watanabe, M., Yamada, T., Takami, H., Usuda, T., & Tamura, M. 2010, *PASJ*, 62, 779
- Nelson, A. F. 2006, *MNRAS*, 373, 1039
- Papaloizou, J. C. B. & Terquem, C. 1995, *MNRAS*, 274, 987
- Price, D. J. & Monaghan, J. J. 2007, *MNRAS*, 374, 1347
- Ratzka, T., Schegerer, A. A., Leinert, C., Ábrahám, P., Henning, T., Herbst, T. M., Köhler, R., Wolf, S., & Zinnecker, H. 2009, *A&A*, 502, 623
- Roccatagliata, V., Ratzka, T., Henning, T., Wolf, S., Leinert, C., & Bouwman, J. 2011, *A&A*, 534, A33
- Tsukamoto, Y. & Machida, M. N. 2011, *MNRAS*, 416, 591
- Tsukamoto, Y. & Makino, J. 2007, *ApJ*, 669, 1316
- Walch, S., Burkert, A., Whitworth, A., Naab, T., & Gritschneider, M. 2009, *MNRAS*, 400, 13
- Walch, S., Naab, T., Whitworth, A., Burkert, A., & Gritschneider, M. 2010, *MNRAS*, 402, 2253
- Walch, S., Whitworth, A. P., & Girichidis, P. 2012, *MNRAS*, 419, 760
- Xie, J.-W., Payne, M. J., Thébault, P., Zhou, J.-L., & Ge, J. 2011, *ApJ*, 735, 10